CRYSTAL GROWTH & DESIGN

Subscriber access provided by Northern Illinois University

Article

Control of Polymorphisms and Functions in All-Inorganic Ionic Crystals based on Polyaluminum Hydroxide and Polyoxometalates

Kosuke Mizuno, Takuto Mura, and Sayaka Uchida

Cryst. Growth Des., **Just Accepted Manuscript** • DOI: 10.1021/acs.cgd.6b00555 • Publication Date (Web): 09 Aug 2016

Downloaded from http://pubs.acs.org on August 15, 2016

Just Accepted

“Just Accepted” manuscripts have been peer-reviewed and accepted for publication. They are posted online prior to technical editing, formatting for publication and author proofing. The American Chemical Society provides “Just Accepted” as a free service to the research community to expedite the dissemination of scientific material as soon as possible after acceptance. “Just Accepted” manuscripts appear in full in PDF format accompanied by an HTML abstract. “Just Accepted” manuscripts have been fully peer reviewed, but should not be considered the official version of record. They are accessible to all readers and citable by the Digital Object Identifier (DOI®). “Just Accepted” is an optional service offered to authors. Therefore, the “Just Accepted” Web site may not include all articles that will be published in the journal. After a manuscript is technically edited and formatted, it will be removed from the “Just Accepted” Web site and published as an ASAP article. Note that technical editing may introduce minor changes to the manuscript text and/or graphics which could affect content, and all legal disclaimers and ethical guidelines that apply to the journal pertain. ACS cannot be held responsible for errors or consequences arising from the use of information contained in these “Just Accepted” manuscripts.

ACS Publications

Crystal Growth & Design is published by the American Chemical Society. 1155 Sixteenth Street N.W., Washington, DC 20036

Published by American Chemical Society. Copyright © American Chemical Society. However, no copyright claim is made to original U.S. Government works, or works produced by employees of any Commonwealth realm Crown government in the course of their duties.

Control of Polymorphisms and Functions in All-Inorganic Ionic Crystals based on Polyaluminum Hydroxide and Polyoxometalates

Kosuke Mizuno,[†,‡] *Takuto Mura,*[†,‡] *and Sayaka Uchida*[†,§,*]

[†]Department of Basic Sciences, School of Arts and Sciences, The University of Tokyo, 3-8-1 Komaba, Meguro-ku, Tokyo 153-8902, Japan.

[§]JST-PRESTO, 4-1-8 Honcho, Kawaguchi, Saitama 332-0012, Japan.

Abstract

Two kinds of polymorphs of all-inorganic ionic crystals were obtained by the combination of oppositely charged molecular ions (macroions) with T_d symmetry, Keggin-type polyaluminum hydroxide $[\varepsilon\text{-Al}_{13}O_4(OH)_{24}(H_2O)_{12}]^{7+}$ (**Al13**) and polyoxometalates (POMs) $[\alpha\text{-CoW}_{12}O_{40}]^{6-}$ (**POM6**), $[\alpha\text{-1,2,3-SiV}^{V}{}_3W_9O_{40}]^{7-}$ (**POM7**), or $[\alpha\text{-1,2,3-SiV}^{IV}V^{V}{}_2W_9O_{40}]^{8-}$ (**POM8**), in aqueous solutions. The needle-type crystals were grown by dissolution-recrystallization of the precipitates, which formed immediately by combining **Al13** and POMs. On the other hand, the plate-type crystals were grown by adding inorganic salts (e.g., NaCl) into the aqueous solution containing the needle-type crystals: Dissolution of the needle-type crystals occurred followed by precipitation of the plate-type crystals, which is the more insoluble and stable polymorph with larger numbers

of hydrogen-bonds between the constituent ions. The plate-type crystals possess one-dimensional channels with large apertures (ca. 12 Å × 6 Å), and showed high activities as heterogeneous solid acid catalysts in pinacol rearrangement.

Introduction

Polymorphism is the ability of a solid to exist in more than one crystal structure. Polymorphs can exhibit different physicochemical properties, and one of the long-standing challenges in science is prediction and control of polymorphism.[1-5] In biomineralization, polymorph selection is a key issue for survival: Mollusks selectively deposit a specific polymorph of $CaCO_3$ (calcite or aragonite) under the control of biopolymers.[2,6] Polymorphism of $CaCO_3$ is one of the most studied subjects in crystal engineering because of its abundant existence in biosphere and lithosphere, and its wide industrial applications as fillers and construction materials.[2,6] Polymorphism of TiO_2 has also been a popular topic due to its high photocatalytic activity, high stability, low cost, and low toxicity.[7] Various reaction conditions, such as concentrations of reactants and additives, temperature, solvent have significant influence on the crystallization of these inorganic oxides. In pharmacy, polymorphism of drug substances has been investigated intensively because drug efficacy is strongly related to the solubility and stability of the polymorphs.[4]

Crystal engineering using molecular building blocks is an important line of research to develop general strategies to form molecular crystals with various internal structures (i.e., polymorphs) and functions for applications in gas adsorption, heterogeneous catalysis, etc.[3,5] Various kinds of interactions between the molecular building blocks, such as coordination bonds, hydrogen bonds, ionic interaction, and van der Waals interaction have been explored. Toward this end, molecular ions (macroions) with a Keggin-type structure have been a popular motif because of its easy synthesis and high molecular symmetry (T_d), which may lead to formation of polymorphs with different functions.[8-12] Especially, Keggin-type polyoxometalate anions (POMs), which are nano-sized anionic metal-oxygen clusters of early transition metals, have been stimulating research in broad fields of sciences.[13-16] Kwon *et al.*, have studied the structures and water adsorption properties of porous ionic crystals composed of POMs and Keggin-type polyaluminum hydroxide ($[\varepsilon\text{-}Al_{13}O_4(OH)_{24}(H_2O)_{12}]^{7+}$,[17] **Al13**).[8-10] In one of their studies, two kinds of polymorphs with **Al13** and $[\alpha\text{-}H_2W_{12}O_{40}]^{6-}$ as building blocks crystallized from the same aqueous solution.[10] Mellot-Dranznieks *et al.*, have predicted the crystal structures of polymorphs composed of $[\varepsilon\text{-}PMo_{12}O_{36}(OH)_4]^{7-}$, benzenedicarboxylates, and Zn(II) ions by computational simulations, and some of the polymorphs were actually synthesized and applied as an electrocatalyst for reduction of bromate.[11,12] However, most of the studies involving polymorphism have been carried out with the aid of organic molecules or polymers, which are designed to assist the self-assembly process of building blocks.

According to these considerations, we attempted to control not only the polymorphism but also the functions of all-inorganic porous ionic crystals. Two kinds of polymorphs (needle and plate-type crystals) were obtained by the combination of oppositely charged macroions with T_d symmetry (**Al13** and POMs: $[\alpha\text{-}CoW_{12}O_{40}]^{6-}$ (**POM6)**, $[\alpha\text{-}1,2,3\text{-}SiV^{V}_3W_9O_{40}]^{7-}$ (**POM7**), or $[\alpha\text{-}1,2,3\text{-}SiV^{IV}V^{V}_2W_9O_{40}]^{8-}$ (**POM8**)) in aqueous solutions. The needle-type crystals were grown by dissolution-recrystallization of the precipitates, which formed immediately by combining **Al13** and POMs. The plate-type crystals were obtained by adding inorganic salts (e.g., NaCl) into the aqueous solution containing the needle-type crystals. It is well known in protein crystals that addition of salts can tune the interactions among solute, solvent, and precipitate, and induces polymorphism.[18] Dissolution of the needle-type crystals occurred followed by precipitation of the plate-type crystals, which is the more insoluble and stable polymorph with larger numbers of hydrogen-bonds between the constituent ions. The plate-type crystals possessed one-dimensional channels with large apertures (ca. 12 Å × 6 Å) and showed high activities as heterogeneous solid acid catalysts in pinacol rearrangement.

Experimental Section

Synthesis

The solution containing $[\varepsilon\text{-}Al_{13}O_4(OH)_{24}(H_2O)_{12}]^{7+}$ (**Al_{13}**) was prepared according to ref.19: Into 200 mL of water, 12 g of $AlCl_3 \cdot 6H_2O$ was added (0.25 mol L^{-1} $AlCl_3aq$) and stirred at 353 K (solution A). Into 450 mL of water, 4.5 g of NaOH was added (0.25 mol L^{-1} NaOHaq), and this solution was slowly added to solution A over 15 min under continuous stirring. $K_6[\alpha\text{-}CoW_{12}O_{40}]\cdot nH_2O$ (**POM6**) and $K_6H[\alpha\text{-}1,2,3\text{-}SiV^{V}{}_3W_9O_{40}]\cdot nH_2O$ (**POM7**) were synthesized according to previous reports.[20,21] $K_6H_2[\alpha\text{-}1,2,3\text{-}SiV^{IV}V^{V}{}_2W_9O_{40}]\cdot nH_2O$ (**POM8**) was obtained by reducing $K_6H[\alpha\text{-}1,2,3\text{-}SiV^{V}{}_3W_9O_{40}]\cdot nH_2O$ with aqueous ascorbic acid.

The ionic crystals (**Al_{13}-POMs**) were synthesized as follows: 20 mL of 6.0 mmol L^{-1} aqueous solution of the potassium salts of POM were added to 20 mL of **Al_{13}** solution, followed by immediate and spontaneous formation of precipitates (solution B). Solution B was left under ambient conditions, and needle crystals of **POM6-*N***, **POM7-*N***, and **POM8-*N*** were obtained through dissolution-recrystallization within 3 days (yields were 70−90% based on POM). Alternatively, 20 mL of 6.0 mmol L^{-1} aqueous solution of the potassium salts of POM were added to 20 mL of **Al_{13}** solution containing NaCl (1.2 g (20 mmol) for **POM6** and 2.4 g (40 mmol) for **POM7** and **POM8**) (solution C). Solution C was left under ambient conditions, and plate crystals of **POM6-*P***, **POM7-*P***, and **POM8-*P*** were obtained within 3 days (yields were ca. 70−90% based on POM). **Al_{13}-POMs** were characterized by IR spectroscopy (Figure S1), diffuse-reflectance UV-*vis* spectroscopy (Figure S2), solid state ^{27}Al-MASNMR spectroscopy (Figure S3), thermogravimetry (Figure S4), X-ray photoelectron spectroscopy (XPS) (Figure S5), elemental analysis, and single crystal X-ray diffraction (XRD). The powder XRD patterns of **Al_{13}-POMs** were totally different from the raw materials (Figure S6). Plate-type crystals could be obtained by using additives other than NaCl (Figure S7: LiCl, KCl, RbCl, $AlCl_3$) or by adding NaCl to solution B.

Characterization

Inductively coupled plasma optical emission spectrometry (ICP-OES) (Agilent Technologies, ICP-OES720) was used for the quantitative analysis of inorganic elements. Atomic absorption spectroscopy (AAS) analysis (Hitachi, ZA3000) was used for the quantitative analysis of alkali metals. See Figure S8 for the calibration curves of Na (λ = 589 nm) and K (λ = 766.5 nm). Prior to the ICP-OES and AAS measurements, conc. HNO_3 (1 mL) was added to ca. 10 mg of **Al_{13}-POMs** to dissolve the solid completely into water (100 mL). In order to check the absence of chlorine, XPS was conducted with a JPS-90SX spectrometer (JEOL) equipped with a magnesium anode (Mg Kα = 1253.6 eV) operating at 8 kV-10 mA. IR spectra were measured by KBr pellet method with a JASCO FT/IR 4100 spectrometer (JASCO) equipped with a TGS detector. Diffuse-reflectance UV-*vis* spectra were measured in the range of 12500–40000 cm^{-1} (800–250 nm) with a V-550 UV-*vis* spectrometer (JASCO). The samples were prepared by grinding and diluting the compounds (ca. 10 mg) with ca. 1 g of NaCl. Solid state ^{27}Al and ^{1}H-MASNMR spectra were measured with a Bruker AVANCE III 400 WB spectrometer (Bruker) equipped with a 4 mm standard probe operating at 400.18 MHz and a MAS rate of 10 kHz. Thermogravimetry was conducted with a Thermo Plus 2 thermogravimetric analyzer (Rigaku) with α-Al_2O_3 as a reference under a dry N_2 flow (100 mL min^{-1}) in the temperature range of 303−773 K. Powder XRD patterns were measured with a New advance D8 X-ray diffractometer (Bruker) by using Cu Kα radiation (λ = 1.54056 Å, 40 kV-40 mA) at 1.8 deg min^{-1}. Scanning electron microscope (SEM) images were obtained with JSM-6700F (JEOL) operating at an accelerating voltage of 5 kV. N_2 (77 K) adsorption isotherms were measured using a Belsorp-max volumetric adsorption apparatus (BEL Japan). Prior to the measurement, about 0.1 g of crystals were ground and treated in vacuo at 298 K for 3 h.

Catalytic reaction

Reactions were carried out in a glass reactor equipped with a magnetic stirrer. In a typical run, a mixture of pinacol (2.0 mmol), naphthalene (0.8 mmol, internal standard), and **Al_{13}-POM** (0.2 mmol) in toluene (3 mL) were stirred under air at 373 K. The reaction progress was followed by gas chromatography using a GC-2014 (Shimadzu) fitted with an InertCap 5 capillary column (GL Sciences) and a flame ionization detector. As a reference, $Na[\varepsilon\text{-}Al_{13}O_4(OH)_{24}(H_2O)_{12}](SO_4)_4$ (**Al_{13}-Sulfate**) was synthesized and used as a solid catalyst under the same reaction condition. **Al_{13}-Sulfate** was synthesized according to ref. 19: 250 mL of 0.1 mol L^{-1} Na_2SO_4 was added to 340 mL of Al_{13} solution, and 2.0 g of colorless crystals of **Al_{13}-Sulfate** were obtained after 1 day (see Figure S9 for the crystal structure).

Single-crystal XRD and structure analysis

XRD data were collected at 93 K with a CCD 2D detector by using a Rigaku Mercury diffractometer with graphite-monochromated MoKα radiation (λ = 0.71069 Å). The structures were solved by direct methods (SHELX97), expanded by Fourier techniques, and refined by fullmatrix least-squares against F^2 with the SHELXL-2014 package. PLATON/ SQUEEZE was used in the refinements. CCDC-1456905, 1456906, and 1456907 contains the supplementary crystallographic data for **POM6-*N***, **POM7-*N***, and **POM8-*N***, respectively. CCDC-1465341 contains the supplementary crystallographic data for **POM6-*P***. Void analyses were carried out with a structure visualization program Mercury (CCDC). Single crystals suitable for X-ray structure analysis could not be obtained for **POM7-*P*** and **POM8-*P***. The powder XRD patterns of **POM7-*P*** and **POM8-*P*** were analogous to that of **POM6-*P***, showing that these compounds possess the same porous structure (see results and discussion for the details). Tables S1 and S2 show the selected bond distances and angles for **POM6-*N*** and **POM6-*P***, respectively. Table S3 summarizes the possible hydrogen bonds (O-O < 3.0 Å) and their distances in **POM6-*N*** and **POM6-*P***.

Elemental analysis

According to the results of thermogravimetry (Figure S4) and quantitative analysis of inorganic elements, chemical formulae of **Al_{13}-POMs** were determined as follows. **POM6-*N***: $[\varepsilon\text{-}Al_{13}O_4(OH)_{25}(H_2O)_{11}][\alpha\text{-}CoW_{12}O_{40}]\cdot 34H_2O$, **POM6-*P***: $[\varepsilon\text{-}Al_{13}O_4(OH)_{25}(H_2O)_{11}][\alpha\text{-}CoW_{12}O_{40}]\cdot 42H_2O$, **POM7-*N***: $[\varepsilon\text{-}Al_{13}O_4(OH)_{24}(H_2O)_{12}][\alpha\text{-}1,2,3\text{-}SiV_3W_9O_{40}]\cdot 32H_2O$, **POM7-*P***: $[\varepsilon\text{-}Al_{13}O_4(OH)_{24}(H_2O)_{12}][\alpha\text{-}1,2,3\text{-}SiV_3W_9O_{40}]\cdot 43H_2O$, **POM8-*N***: $[\varepsilon\text{-}Al_{13}O_4(OH)_{24}(H_2O)_{12}][\alpha\text{-}1,2,3\text{-}HSiV_3W_9O_{40}]\cdot 35H_2O$, **POM8-*P***: $[\varepsilon\text{-}Al_{13}O_4(OH)_{24}(H_2O)_{12}][\alpha\text{-}1,2,3\text{-}HSiV_3W_9O_{40}]\cdot 45H_2O$. AAS (K, Na), XPS (Cl), and ion-exchange chromatography (Cl) showed that **Al_{13}-POMs** *do not* contain Na, K, or Cl (see Figures S5 and S8 for the details). Elemental analysis for **POM6-*N*** (calc): Al 8.0 (7.7), Co 1.32 (1.29), W 50.6 (48.4). **POM6-*P***: Al 8.0 (7.5), Co 1.30 (1.25), W 48.9 (46.9). **POM7-*N***: Al 8.8 (8.6), Si 0.64 (0.69), V 3.8 (3.7), W 40.5 (40.4). **POM7-*P***: Al 8.6 (8.2), Si 0.75 (0.65), V 3.9 (3.6), W 39.6 (38.6). P**OM8-*N***: Al 8.2 (8.5), Si 0.68 (0.68), V 3.7 (3.7), W 39.8 (39.9). **POM8-*P***: Al 7.8 (8.1), Si 0.65 (0.68), V 3.7 (3.5), W 38.2 (38.2).

Results and Discussion

Blue *needle-type* crystals of **POM6-*N*** (Figure 1) were grown via dissolution-recrystallization of the precipitate, which formed immediately by mixing the aqueous solution of **Al₁₃** with POM ($[\alpha\text{-CoW}_{12}\text{O}_{40}]^{6-}$). IR (Figure S1) and solid state ^{27}Al-MASNMR (Figure S3) spectra confirmed that the molecular structures of **Al_{13}** and POM were essentially retained in **POM6-*N***.[20-22] The powder XRD pattern of the precipitate was analogous to that of **POM6-*N*** (Figure S10), showing that the structures were basically the same. The crystal structure of **POM6-*N*** (Figure 1 and Table 1) was analogous to that of the ionic crystal composed of **Al_{13}** and $[\alpha\text{-H}_2\text{W}_{12}\text{O}_{40}]^{6-}$ reported by Kwon *et al*.[10,23] In the crystal structure of **POM6-*N***, **Al_{13}** and POM were arranged alternately in a tetragonal cell by electrostatic interactions and hydrogen bonds. Straight channels existed along the [001], [110], and [1-10] directions, which were interconnected to each other. The minimum aperture of the channel was ca. 6 Å × 6 Å. Elemental analysis and thermogravimetry (Figure S4) suggested that **POM6-*N*** contained about 34 mol mol^{-1} of water of crystallization. Single crystal X-ray structure analysis could locate 25 mol mol^{-1} of water molecules, which existed in the channels and were hydrogen-bonded to other water molecules and/or to the constituent ions.

When NaCl was added to the aqueous mixture of **Al_{13}** and POM, the precipitate dissolved completely and blue *plate-type* crystals of **POM6-*P*** were formed (Figure 1 and Table 1). Elemental analysis and single crystal X-ray structure analysis showed that **POM6-*P*** and **POM6-*N*** are *polymorphs*. **POM6-*P*** crystallized in an orthorhombic cell, **Al_{13}** and POM each formed columns along the *a*-axis, and these columns lined up along the *c*-axis by electrostatic interactions and hydrogen bonds. Two-dimensional layers were formed in the *ac*-plane, which stacked along the *b*-axis, and disordered POMs existed in the interlayer space. As a result, one-dimensional channels existed along the *a*-axis with a minimum aperture of ca. 6 Å × 12 Å. Elemental analysis and thermogravimetry (Figure S4) suggested that **POM6-*P*** contained 42 mol mol^{-1} of water of crystallization, while only 14.5 out of 42 mol mol^{-1} could be located with single crystal X-ray structure analysis. The water of crystallization existed in the channels and were hydrogen-bonded to other water molecules and/or to the constituent ions. Notably, **POM6-*P*** could be obtained with additives other than NaCl (see Figure S7 for the powder XRD patterns of the products). The effects of the additives will be discussed later.

Synthesis of porous ionic crystals was also carried out with other POMs having negative charges of 7 ($[\alpha\text{-}1,2,3\text{-SiV}^{V}_{3}W_9O_{40}]^{7-}$) or 8 ($[\alpha\text{-}1,2,3\text{-SiV}^{IV}V^{V}_{2}W_9O_{40}]^{8-}$), which resulted in the formation of orange and black crystals of **POM7-*N*** and **POM8-*N***, respectively. The powder XRD patterns of **POM6-*N***, **POM7-*N***, and **POM8-*N*** (Figure 2a-d) were analogous. The crystal structures of **POM7-*N*** and **POM8-*N*** were solved by single crystal X-ray analysis (Table 1). Synthesis of polymorphs was also attempted by adding NaCl to the synthetic solutions of **POM7-*N*** and **POM8-*N***, which resulted in the formation of **POM7-*P*** and **POM8-*P***, respectively. The powder XRD patterns of **POM6-*P***, **POM7-*P***, and **POM8-*P*** (Figure 2e-h) were analogous. These results show that anion charge has little effect toward the crystal structure in the range of −6 to −8.[24,25]

The crystal structures of the polymorphs were studied in detail. Figure 3a shows the void analysis of **POM6-*N*** with a probe diameter of 4 Å (grid spacing 0.5 Å). Water of crystallization was removed from the structure and hydrogen atoms of **Al$_{13}$** were geometrically added to improve the accuracy of estimation. The void volume was 24.3% (2365 Å^3 per unit cell, Z = 4) of the unit cell volume. As described above, straight channels exist along the [001], [110], and [1-10] directions, which were interconnected to each other, and the minimum aperture was ca. 6 Å × 6 Å. Figures 3b and 3c show the local structures and possible hydrogen bonds between the molecular ions of **POM6-*N***. A **Al$_{13}$** cluster is surrounded by four POMs in a tetrahedral arrangement, and each POM has three hydrogen bonds (O-O distance of < 3.0 Å) with the **Al$_{13}$** cluster (see Table S3 for the distances). Therefore, the total number of hydrogen bonds per **Al$_{13}$** in **POM6-*N*** is twelve.

Void analysis of **POM6-*P*** was carried out by the same method (Figure 4a). The void volume was 21.6% (8311 Å^3 per unit cell, Z = 16) of the unit cell, which is slightly smaller than that of **POM6-*N*** (24.3%) because of the disordered POMs. In contrast to **POM6-*N*** with interconnected three-dimensional channels, **POM6-*P*** possesses one-dimensional channels along the *a*-axis with a minimum aperture of ca. 6 Å × 12 Å. Figures 4b and 4c show the local structures and possible hydrogen bonds between the molecular ions of **POM6-*P***. As shown in Figure 4b, a **Al$_{13}$** cluster has two POMs and two **Al$_{13}$** in the nearest neighbors. There are three and two hydrogen bonds between **Al$_{13}$**-POM and **Al$_{13}$-Al$_{13}$**, respectively. In addition, the **Al$_{13}$** cluster has ten hydrogen bonds with the disordered POMs (Figure 4c) (see Table S3 for the distances).[26] Therefore, the total number of hydrogen bonds per **Al$_{13}$** in **POM6-*N*** is twenty, which is larger than that of **POM6-*N*** (twelve).

The powder XRD patterns of **POM6-*N*** and **POM6-*P*** broadened after evacuation at rt (Figure S11), showing that water of crystallization are necessary to maintain the porous structure. The crystal structures can be restored by exposure to water vapor. **POM6-*N*** and **POM6-*P*** showed low porosity and BET surface area based on N_2 adsorption at 77 K (Figure S12), in accordance with the broad powder XRD patterns. However, we[16] and other groups[27,28] have reported that such kind of host-guest systems also show interesting properties in guest-exchange, proton conduction, acid catalysis, etc.

The polymorphs were utilized as heterogeneous solid acid catalysts in pinacol rearrangement (Scheme 1), which is a typical acid reaction.[29] **Al_{13}** exhibits acidity and has been used as a pillar in clay-supported catalysts.[30,31] Table 2 summarizes the results of pinacol rearrangement with **Al_{13}-POMs** as heterogeneous solid catalysts at 373 K. The catalytic activities of the raw materials (**Al_{13}-sulfate**, **POM6**, **POM7**, and **POM8**) were low (conv. 4−8%, yield of pinacolone 2−5%), which is probably due to the non-porous structure so that reaction occurs only at the particle surface (Figure S9).[32] The catalytic activities of needle-type crystals (conv. 21−31%, yield of pinacolone 8−18%) were higher than that of **Al_{13}-sulfate**, suggesting that pinacol molecules could enter the porous structure. Acetone was formed by the oxidative dissociation of pinacol, which is probably due to the reduction of vanadium moieties in **POM7-*N*** and **POM8-*N***. Notably, the catalytic activities of plate-type crystals (conv. 45−76%, yield of pinacolone 26−54%) were higher than those of the needles, suggesting that channels with large apertures (ca. 6 Å × 12 Å and ca. 6 Å × 6 Å for the plates and needles, respectively) is favorable.[33] The powder XRD pattern of **POM6-*P*** after the reaction (Figure 2i) was analogous to that before the reaction (Figure 2f), showing that crystal structure of the catalyst is maintained during the reaction. SEM images of **POM6-*N*** and **POM6-*P*** before and after the reaction (Figure S13) were similar, suggesting that particle size does not affect the catalytic activities.

The high catalytic activities of plate-type crystals may be due to not only the large aperture of channels but also high acid strength. In order to characterize acidity, solid state ^{1}H-MASNMR spectroscopy was utilized. It is well established that strengths of Brønsted acid sites increase with increase in chemical shift of the solid state ^{1}H-MASNMR signal.[34] ^{1}H-MASNMR spectra of

POM6-*N* and **POM6-*P*** with **Al_{13}-sulfate** as a reference are shown in Figure 5. Both polymorphs gave a single signal at 4.7 ppm, showing that the states of protons and thus the acidity are essentially the same. The lower chemical shift compared with **Al_{13}-sulfate** (5.4 ppm) is probably due to the leveling effect[35] caused by the large amounts of water of crystallization in the channels. These results suggest that the high catalytic activity of the plate-type crystals is due to the large aperture of the channels, so that pinacol molecules may enter and diffuse through the porous structure smoothly and **Al_{13}** exposed to the inner pore surface could participate in the reaction.

Finally, the effects of additives toward the formation of polymorphs were considered in the case of **POM7-*N*** and **POM7-*P***. When NaCl was added to the aqueous mixture containing **POM7-*N***, **POM7-*N*** dissolved followed by crystallization of **POM7-*P***. Figure S14 shows the photo images of **POM7-*N*** in aqueous solutions of sodium salts (NaCl, Na_2SO_4 or Na_2CO_3). The solution is colorless and transparent without any sodium salts showing that **POM7-*N*** is insoluble in water. On the other hand, the solutions turned orange and turbid by the addition of sodium salts, showing that **POM7-*N*** dissolved back into the solution. Focusing on the types of anion of the sodium salts, turbidity of the solution or solubility of **POM7-*N*** increased in the order of $Cl^- < SO_4^{2-} < CO_3^{2-}$, which is in line with the hardness of the anions as a Lewis base. Figure S15 shows the photo images of **POM7-*N*** in aqueous solutions of chlorides (KCl, NaCl, or $CaCl_2$). The solutions turned orange and turbid by the addition of chlorides, showing that **POM7-*N*** dissolved back into the solution. Focusing on the types of cation of the chlorides, turbidity of the solution or solubility of **POM7-*N*** increased in the order of $K^+ < Na^+ < Ca^{2+}$, which is also in line with the hardness of the cations as a Lewis acid.

According to these observations, the formation of polymorphs can be explained qualitatively as follows: Anions and cations of the additives interact with the needle-type crystals via electrostatic interaction, shield the attractive interaction between the constituent ions (**Al_{13}** and POMs), and the constituent ions would peel off from the crystals causing dissolution. The plate-type crystals crystallize subsequently, which is the more insoluble and probably stable form with larger numbers of hydrogen bonds between the constituent ions.

Conclusion

Two kinds of polymorphs of all-inorganic ionic crystals were obtained by the combination of oppositely charged macroions with T_d symmetry (**Al_{13}** and POMs) in aqueous solutions. The needle-type crystals were grown by dissolution-recrystallization of the precipitates, which formed immediately by combining **Al_{13}** and POMs. On the other hand, the plate-type crystals were grown by adding inorganic salts into the aqueous solution containing the needle-type crystals: Dissolution of the needle-type crystals occurred followed by precipitation of the plate-type crystals, which is the more insoluble and stable polymorph with larger numbers of hydrogen-bonds between the constituent ions. The plate-type crystals possess one-dimensional channels with large apertures (ca. 12 Å × 6 Å), and showed high activities as heterogeneous solid acid catalysts in pinacol rearrangement. *All these results show the control of polymorphism and functions in all-inorganic porous ionic crystals.*

Supporting Information

Table S1: Selected bond distances and angles for **POM6-*N***. Table S2: Selected bond distances and angles for **POM6-*P***. Table S3: Possible hydrogen-bonds (O-O < 3.0 Å) and their distances in **POM6-*N*** and **POM6-*P***. Table S4: Pinacol to pinacolone rearrangement over various solid catalysts and conditions. Figure S1: IR spectra. Figure S2: Diffuse-reflectance UV-*vis* spectra. Figure S3: Solid state ^{27}Al-MASNMR spectra. Figure S4: Thermogravimetry. Figure S5: Wide scan XPS spectra. Figure S6: Powder XRD patterns of **Al_{13}-POMs** (**POM6-*P*** and **POM6-*N***) and the raw materials. Figure S7: Powder XRD patterns of **POM6-*P*** synthesized with additives other than NaCl. Figure S8: Calibration curves of (a) Na (λ = 589 nm) and (b) K (λ = 766.5 nm) in AAS. Figure S9: Crystal structure of **Al_{13}-sulfate**. Figure S10: Powder XRD patterns of the precipitate and the needle crystal (**POM6-*N***). Figure S11: Powder XRD patterns of **POM6-*N*** and **POM6-*P*** before and after evacuation. Figure S12: N_2 adsorption isotherms (77 K). Figure S13: SEM images. Figure S14: Effects of anions of additives. Figure S15: Effects of cations of additives.

Corresponding Author

Sayaka Uchida, e-mail csayaka@mail.ecc.u-tokyo.ac.jp

Author Contributions

The manuscript was written through contributions of all authors. All authors have given approval to the final version of the manuscript. [‡]These authors contributed equally.

Notes

The authors declare no competing financial interest.

Acknowledgements

This work was supported by JST-PRESTO and Grant-in-Aids for Scientific Research from the Ministry of Education, Culture, Science, Sports, and Technology of Japan. Prof. Motoyuki Matsuo and Dr. Katsumi Shozugawa (Univ. of Tokyo) are acknowledged for providing access to the ICP instrument. Members of Prof. Noritaka Mizuno group (Univ. of Tokyo) are acknowledged for providing access to the XPS and DLS instruments. Prof. Junko N. Kondo and Mr. Ryota Osuga are acknowledged for the preliminary IR measurements to characterize the acid sites.

References and Notes

(1) Bernstein, J. *Cryst. Growth and Des.* **2011**, *11*, 632-650.

(2) Cartwright, J. H. E.; Checa, A. G.; Gale, J. D.; Gebauer, D.; Sainz-Diaz, C. I. *Angew. Chem. Int. Ed.* **2012**, *51*, 11960-11970.

(3) Desiraju, G. R. *Angew. Chem. Int. Ed.* **2007**, *46*, 8342-8356.

(4) Pudipeddi, M.; Serajuddin, A. T. M. *J. Pharm. Sci.* **2005**, *94*, 929-939.

(5) Moulton, B.; Zaworotko, M. J. *Chem. Rev.* **2001**, *101*, 1629-1658.

(6) Xu, A. –W.; Dong, W. –F; Antonietti, M.; Cölfen, H. *Adv. Funct. Mater.* **2008**, *18*, 1307-1313.

(7) Hanaor, D. A. H.; Sorrell, C. C. *J. Mater. Sci.* **2011**, *46*, 855-874.

(8) Son, J. –H.; Choi, H.; Kwon, Y. –U. *J. Am. Chem. Soc.* **2000**, *122*, 7432-7433.

(9) Son, J. –H.; Kwon, Y. –U. *Inorg. Chem.* **2004**, *43*, 1929-1932.

(10) Son, J. –H.; Kwon, Y. –U. *Inorg. Chim. Acta.* **2005**, *358*, 310-314.

(11) Rodriguez-Albelo, L. M.; Ruiz-Salvador, A. R.; Sampieri, A.; Lewis, D. W.; Gómez, A.; Nohra, B.; Mialane, P.; Marrot, J.; Sécheresse, F.; Mellot-Draznieks, C.; Biboum, R. N.; Keita, B.; Nadjo, L.; Dolbecq, A. *J. Am. Chem. Soc.* **2009**, *131*, 16078-16087.

(12) Rodriguez-Albelo, L. M.; Ruiz-Salvador, A. R.; Lewis, D. W.; Gómez, A.; Mialane, P.; Marrot, J.; Dolbecq, A.; Sampieri, A.; Mellot-Draznieks, C. *Phys. Chem. Chem. Phys.* **2010**, *12*, 8632-8639.

(13) Hill, C. L. Ed. Thematic Issue on Polyoxometalates, *Chem. Rev.* **1998**, *98*, 1-390.

(14) Cronin, L.; Müller, A. Eds. Thematic Issue on Polyoxometalates, *Chem. Soc. Rev.* **2012**, *41*, 7325-7648.

(15) Seino, S.; Kawahara, R.; Ogasawara, Y.; Mizuno, N.; Uchida, S. *Angew. Chem. Int. Ed.* **2016**, *55*, 3987-3991.

(16) Kawahara, R.; Niinomi, K.; Kondo, J. N.; Hibino, M.; Mizuno, N.; Uchida, S. *Dalton Trans.* **2016**, *45*, 2805-2809.

(17) Casey, W. H. *Chem. Rev.* **2006**, *106*, 1-16.

(18) Gillespie, C. M.; Asthagiri, D.; Lenhoff, A. M.; *Cryst. Growth and Des.* **2014**, *14*, 46-57.

(19) Wang, M.; Muhammed, M. *Nanostr. Mat.* **1999**, *11*, 1219-1229.

(20) Baker, L. C. *J. Am. Chem. Soc.* **1959**, *81*, 4744.

(21) Domaille, P. J. *J. Am. Chem. Soc.* **1984**, *106*, 7677-7687.

(22) Bradley, S. M.; Kydd, R. A.; Fyfe, C. A. *Inorg. Chem.* **1992**, *31*, 1181-1185.

(23) Because of the charge-mismatch between **Al13** (+7) and $[\alpha\text{-CoW}_{12}O_{40}]^{6-}$ (−6), **POM6-*N*** can be formulated as $[\varepsilon\text{-Al}_{13}O_4(OH)_{24}(H_2O)_{12}][\alpha\text{-CoW}_{12}O_{40}](OH)\cdot 26H_2O$ with a hydroxide ion as in ref. 10 or as $[\varepsilon\text{-Al}_{13}O_4(OH)_{25}(H_2O)_{11}][\alpha\text{-CoW}_{12}O_{40}]\cdot 26H_2O$. Synthetic solution of **POM6-*N*** is acidic (pH = 4), so we decided that the inclusion of a hydroxide ion in the formula is inappropriate in our case.

(24) Because of the charge-mismatch between **Al_{13}** (+7) and $[\alpha\text{-}1,2,3\text{-}SiV^{IV}V^{V}_{2}W_9O_{40}]^{8-}$ (−8) in **POM8-*N*** and **POM8-*P***, a proton (H^+) was added to the formula.

(25) Ionic crystals could not be obtained with Keggin-type POMs of $[\alpha\text{-}BW_{12}O_{40}]^{5-}$, $[\alpha\text{-}SiW_{12}O_{40}]^{4-}$, or $[\alpha\text{-}PW_{12}O_{40}]^{3-}$.

(26) According to Figure 4a, there are nine hydrogen-bonds between **Al_{13}** and the disordered POM. There is another disordered POM beneath the **Al_{13}**, so there are eighteen hydrogen-bonds between **Al_{13}** and the disordered POM. Out of the nine oxygen atoms of POM, which are in hydrogen-bonding distances with the **Al_{13}**, one and eight oxygen atoms have occupancies of 1 and 0.5, respectively. Therefore, there are $1 \times 2 + 0.5 \times 16 = 10$ hydrogen-bonds between **Al_{13}** and the disordered POMs.

(27) Biradha, K.; Dennis, D.; MacKinnon, N. K. R.; Sharma V. K.; Zaworotko, M. J. *J. Am. Chem. Soc.* **1998**, *120*, 11894-11903.

(28) Wang, H.; Xu, X.; Johnson, N. M.; Dandala N. K. R.; Ji, H. F. *Angew. Chem. Int. Ed.* **2011**, *50*, 12538-12541.

(29) Pinacol to pinacolone rearrangement over various solid catalysts and conditions are summarized in Table S4. Note that there are many superior catalysts for this reaction. In this work, catalytic reaction was utilized as a characterization.

(30) Pinnavaia, T. J.; Tzou, M. –S.; Landau, S. D.; Raythatha, R. H. *J. Mol. Catal.* **1984**, *27*, 195-212.

(31) Kooli, F. *Micropor. Mesopor. Mat.* **2014**, *184*, 184-192.

(32) The reaction also proceeded with the POMs as catalysts because partial dissolution of the POMs was observed and acidic protons were contained in **POM7** and **POM8**.

(33) Note that the carbon balances (total yield / conv.) of the plate-type crystals were about 90%, probably because relatively large amounts of reactant and products were absorbed in the catalysts.

(34) Freude, D.; Hunger, M.; Pfeifer, H. *Chem. Phys. Lett.* **1986**, *128*, 62-66.

(35) Atkins, P. W. Shriver and Atkins' Inorganic Chemistry, Fifth Edition, Oxford University Press, **2010**, Chap. 4.

Table 1. Crystal data

	POM6-*N*	**POM7-*N***	**POM8-*N***	**POM6-*P***
Crystal system	Tetragonal	Tetragonal	Tetragonal	Orthorhombic
Space group	$P4_2/ncm$	$P4_2/ncm$	$P4_2/ncm$	*Ibca*
Unit cell dimensions	a = 18.583(3) c = 28.121(5)	a = 18.559(12) c = 27.896(16)	a = 18.567(5) c = 27.942(8)	a = 26.659(5) b = 31.288(6) c = 46.176(9)
Volume	9711(3)	9608(10)	9633(4)	38515(13)
Z	4	4	4	16
D_{calc} (g cm^{-3})	3.116	2.828	2.859	3.131
F(000)	8444	7704	7828	33766
h, k, l range	–21/22, –19/22, –33/33	–23/24, –23/24, –34/36	–23/20, –23/23, –34/34	–27/32, –37/37, –51/55
μ (Mo Kα) (mm^{-1})	14.597	11.294	11.270	14.719
$R_1(I > 2\sigma(I))$	0.1243	0.1509	0.1453	0.1479
wR_2 (all data)	0.2982	0.2933	0.3030	0.3591
GOF on F^2	1.145	1.203	1.181	1.121

Table 2. Pinacol rearrangement reaction[a]

Catalyst	Conv. [%]	Yield [%][b]		
		pinacolone	2,3-dimethyl -1,3-butadiene	acetone
POM6-*N*	31	18	13	0
POM7-*N*	22	8	4	9
POM8-N	21	12	5	2
POM6-*P*	76	54	15	0
POM7-*P*	72	26	14	24
POM8-*P*	45	32	5	3
POM6	6	5	1	0
POM7	8	2	1	3
POM8	8	2	2	2
Al_{13}-sulfate	4	2	1	0

[a]Reaction conditions: pinacol (2.0 mmol), naphthalene (0.8 mmol, internal standard), and catalyst (0.2 mmol) in toluene (3 mL) at 373 K, 40 h. [b]Only pinacolone, 2,3-dimethyl-1,3-butadiene, and acetone were detected as products.

Scheme 1 Pinacol rearrangement. Pinacolone is the main product. 2,3-dimethyl-1,3-butadiene (formed via dehydration) and acetone (formed via dissociative oxidation) are by-products.

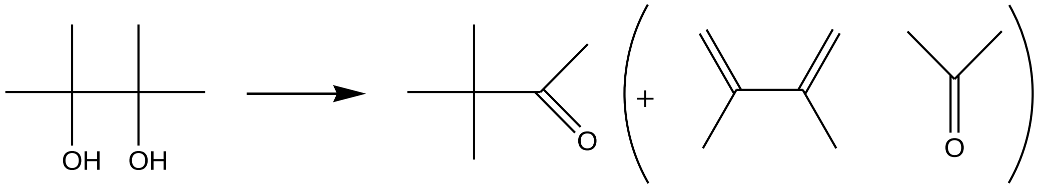

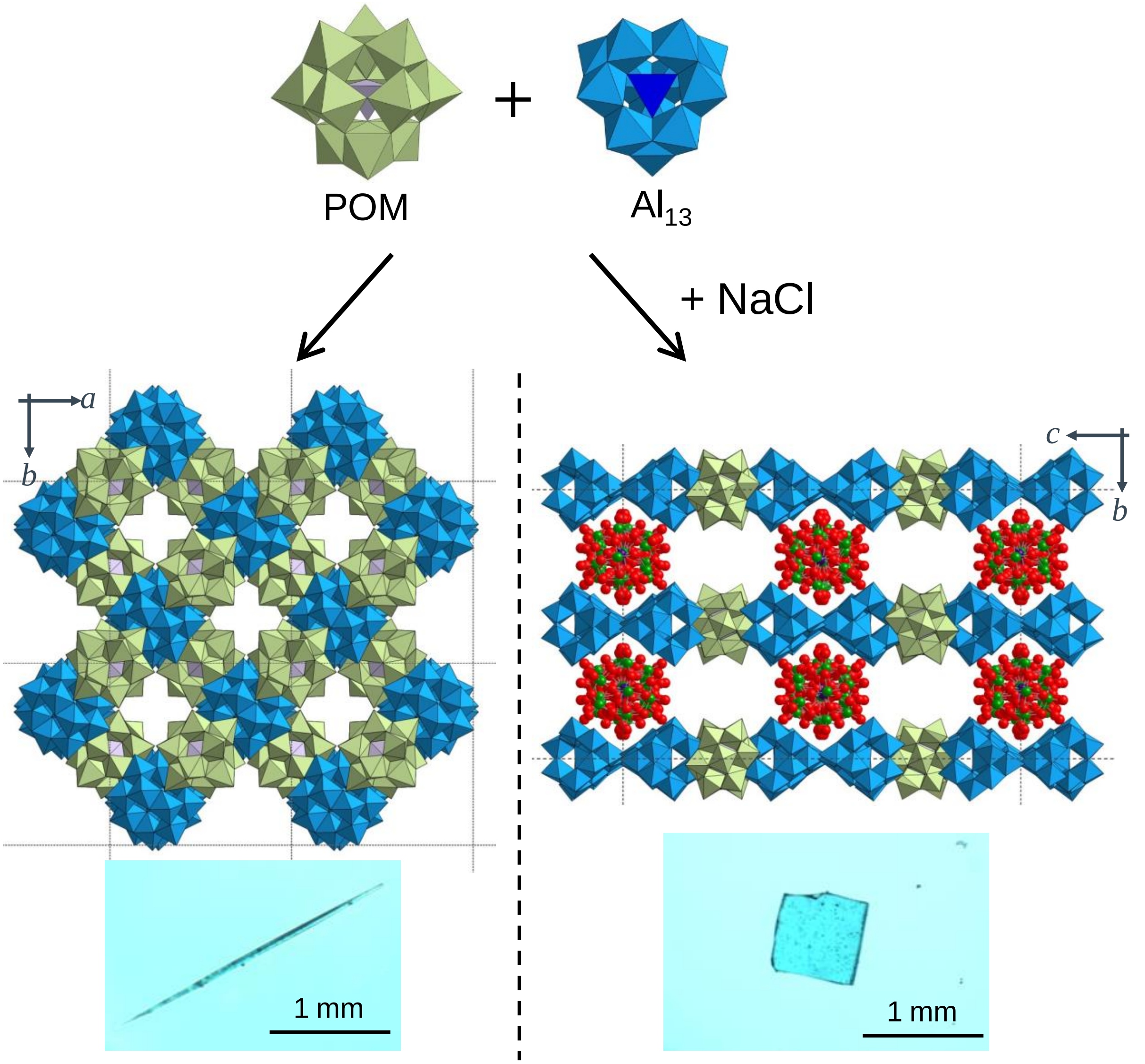

Figure 1. Molecular structures of **Al_{13}** and POM. Crystal structures and photo images of ***POM6-N*** (left) and ***POM6-P*** (right). Green, purple, light blue, and dark blue polyhedra show the [WO_6], [CoO_4], [AlO_6], and [AlO_4] units, respectively. The disordered POMs in ***POM6-P*** are depicted with a ball-and-stick model, where red, green, and purple spheres show the oxygen, tungsten, and cobalt atoms, respectively.

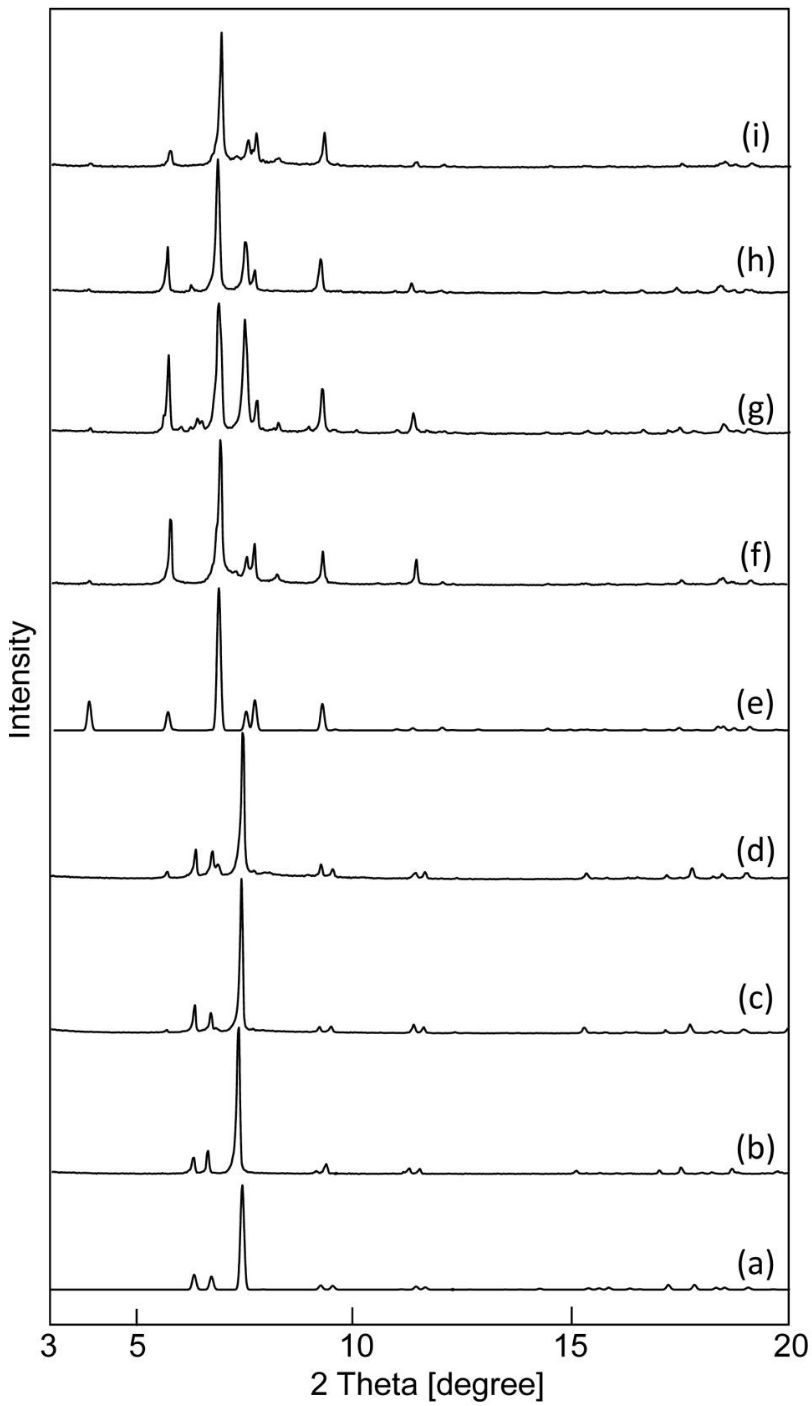

Figure 2. Powder XRD patterns of (a) **POM6-*N*** (calc), (b) **POM6-*N*** (exp), (c) **POM7-*N*** (exp), (d) **POM8-*N*** (exp), (e) **POM6-*P*** (calc), (f) **POM6-*P*** (exp), (g) **POM7-*P*** (exp), (h) **POM8-*P*** (exp), and (i) **POM6-*P*** (exp, after catalytic reaction) .

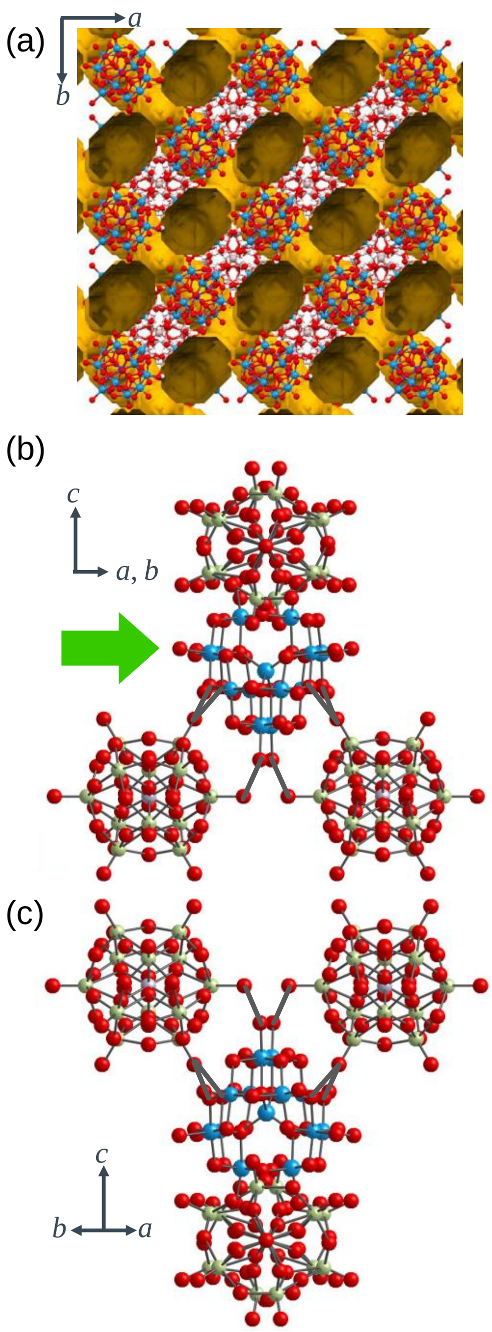

Figure 3. (a) Void analysis of **POM6-*N*** (probe diameter 4 Å, grid spacing 0.5 Å). Voids are shown in brown. Water of crystallization was removed from the crystal structure and hydrogen atoms of **Al_{13}** were geometrically added to the molecular structure. Minimum aperture of the void is ca. 6 Å × 6 Å. Possible hydrogen-bonds (O–O < 3.0 Å, shown by the gray lines) among the building blocks in **POM6-*N*** in the (b) (1−1 0) and (c) (1 1 0) planes. Note that (c) is the view along the green arrow in (b).

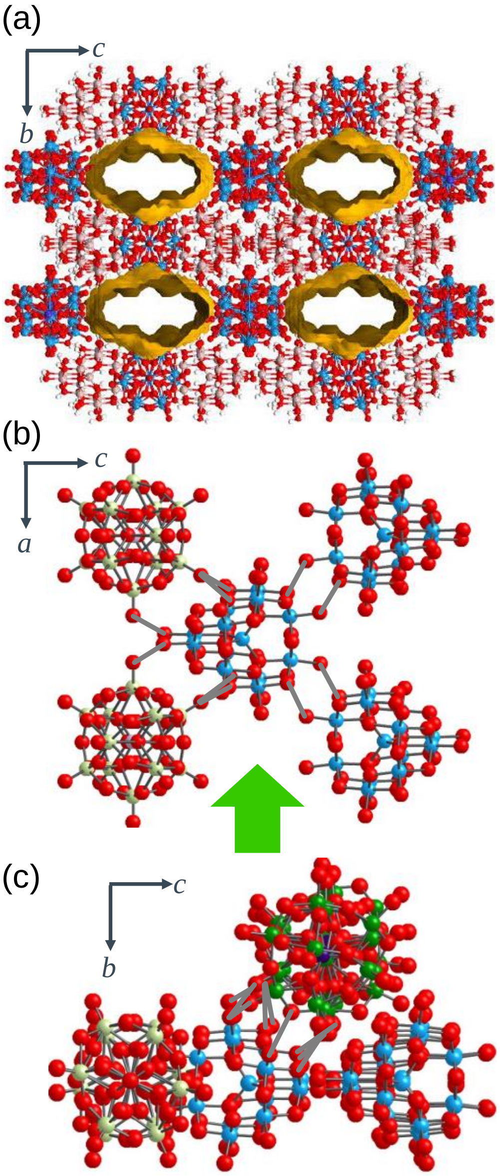

Figure 4. (a) Void analysis (probe diameter 4 Å, grid spacing 0.5 Å) of **POM6-*P***. Voids are shown in brown. Water of crystallization was removed from the crystal structure and hydrogen atoms of **Al$_{13}$** were geometrically added to the molecular structure. The minimum aperture of the void is ca. 6 Å × 12 Å. Possible hydrogen-bonds (O-O < 3.0 Å, shown by the gray lines) among the building blocks in **POM6-*P*** in the (b) (1 0 1) and (c) (0 1 1) planes. Note that (c) is the view along the green arrow in (b). In (c), another disordered POM exists beneath **Al$_{13}$**, which is omitted for the clarity.

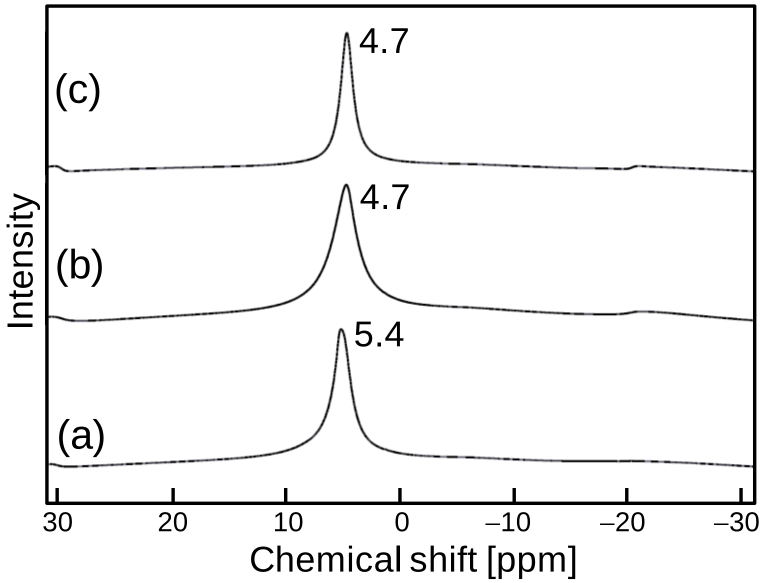

Figure 5. Solid state ^{1}H-MASNMR spectra (MAS = 10 kHz) of (a) **Al$_{13}$-sulfate**, (b) **POM6-*N***, and (c) **POM6-*P***.

For Table of Contents Use Only

Control of Polymorphisms and Functions in All-Inorganic Ionic Crystals based on Polyaluminum Hydroxide and Polyoxometalates

Kosuke Mizuno,†,‡ Takuto Mura,†,‡ and Sayaka Uchida†,§,*

Two kinds of polymorphs were obtained by the combination of oppositely charged molecular ions with T_d symmetry in aqueous solutions. The plate-type crystal was obtained by using additives, and is the stable polymorph with larger numbers of hydrogen-bonds between the molecular ions. The plate-type crystal possesses one-dimensional channels with large openings and showed high activity as a solid catalyst.